Protein Conformational Changes of *Agrobacterium* Phytochrome Agp1 during Chromophore Assembly and Photoconversion†

Steffi Noack,‡ Norbert Michael,‡ Ran Rosen,§,|| and Tilman Lamparter*,‡

Pflanzenphysiologie, Freie Universität Berlin, Königin Luise Strasse 12-16, D-14195 Berlin, Germany, and The Maiman Institute for Proteome Research, The George S. Wise Faculty of Life Sciences, Tel Aviv University, Ramat Aviv, Tel Aviv 69978, Israel

Received November 22, 2006; Revised Manuscript Received January 26, 2007

ABSTRACT: Phytochromes are widely distributed photochromic biliprotein photoreceptors. Typical bacterial phytochromes such as *Agrobacterium* Agp1 have a C-terminal histidine kinase module; the N-terminal chromophore module induces conformational changes in the protein that lead to modulation of kinase activity. We show by protein cross-linking that the C-terminal histidine kinase module of Agp1 mediates stable dimerization. The fragment Agp1-M15, which comprises the chromophore module but lacks the histidine kinase module, can also form dimers. In this fragment, dimer formation was stronger for the far-red-absorbing form Pfr than for the red-absorbing form Pr. The same or similar behavior was found for Agp1-M15Δ9N and Agp1-M15Δ18N, which lack 9 and 18 amino acids of the N-terminus, respectively. The fragment Agp1-M20, which is derived from Agp1-M15 by truncation of the C-terminal "PHY domain" (191 amino acids), can also form dimers, but dimerization is independent of irradiation conditions. The cross-linking data also showed that the PHY domain is in tight contact with Lys 16 of the protein and that the nine N-terminal amino acids mediate oligomer formation. Limited proteolysis shows that the hinge region between the chromophore module and the histidine kinase and a part of the PHY domain become exposed upon Pr to Pfr photoconversion.

Phytochromes are photoreceptors that have been found in plants, bacteria, and fungi and that are most sensitive in the red and far-red region of the visible spectrum (*1*). In plants, numerous photomorphogenetic processes such as de-etiolation, seed germination, and induction of flowering are controlled by phytochromes (*2*). In bacteria, phytochrome primary structures and biological functions are more diverse. The most prominent phytochrome effects were found for the photosynthetic bacteria *Bradyrhizobium* ORS274 and *Rhodopseudomonas palustris*, in which phytochrome controls the synthesis of bacteriochlorophyll and carotenoids (*3*, *4*). The genome of the soil bacterium *Agrobacterium tumefaciens* (*5*, *6*) contains two phytochrome genes. These phytochromes, termed Agp1 and Agp2, have been used for studies of chromophore assembly, photoconversion, and X-ray crystallography (*7*−*15*). Both phytochromes are expressed in *Agrobacterium* at a concentration of 10−20 molecules per cell (*16*). Double-knockout mutants have a reduced growth rate in darkness and light, but details of signal transduction of these phytochromes are as yet unknown (*16*).

All typical phytochrome proteins consist of two parts, the N-terminal chromophore module and a C-terminal output module (*1*). The chromophore module consists of a PAS domain[1] [named for period, ARNT, and single-minded proteins (*17*)] or a PAS-like domain (PLD), a GAF [named for cGMP-specific phosphodiesterase, adenylate cyclase, and Fhl proteins (*18*)] domain and a PHY (specific for photochromic phytochromes) domain, which is located between the C-terminus and the GAF domain. The C-terminal output module of bacterial phytochromes is often a histidine kinase, but other motifs are also possible. Plant phytochromes have a C-terminal histidine kinase-like module and an additional ∼300-amino acid region, termed the double-PAS domain here, which contains two PAS domains and is located between the chromophore module and the histidine kinase-like C-terminus (*1*). The histidine kinase (like) module of plant and bacterial phytochromes also functions as a dimerization unit (*1*), although dimerization has been shown for few phytochromes only. The domain structure of *Agrobacterium* phytochrome Agp1, which was used in this study, is given in Figure 1.

Phytochromes use one of three different bilins as a chromophore for light absorption, which is autocatalytically assembled with the protein. Plant phytochromes incorporate

† This work was supported by Deutsche Forschungsgemeinschaft, Sfb 498, TP B2 (T.L.), and by a Peikovsky Valachi Post Doctoral Fellowship (R.R.).

* To whom correspondence should be addressed. Telephone: +49 (0)30 838 54918. Fax: +49(0)30 838 84357. E-mail: lamparte@zedat.fu-berlin.de.

‡ Freie Universität Berlin.

§ Tel Aviv University.

|| Current address: Agentek (1987) Ltd., Atidim Scientific Park, Tel Aviv, Israel.

[1] Abbreviations: BV, biliverdin; GAF domain, abbreviation derived from cGMP-specific phosphodiesterases, cyanobacterial adenylate cyclases, and transcription activator FhlA; PAS domain, abbreviation derived from PER ARNT SIM; PLD, PAS-like domain; Pfr, far-red-absorbing form of phytochrome; Pr, red-absorbing form of phytochrome; SEC, size exclusion chromatography.

10.1021/bi602419x CCC: $37.00
Published on Web 03/03/2007

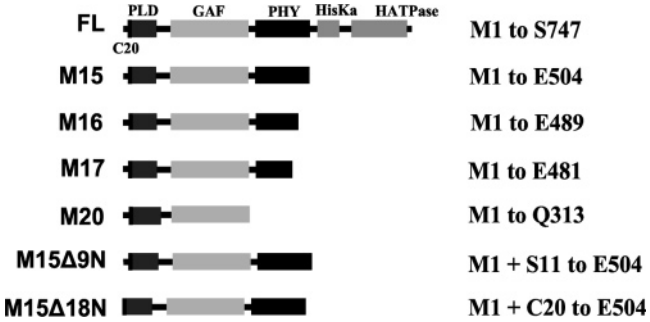

FIGURE 1: Nomenclature and domain structure of the Agp1 fragments used herein. All proteins are expressed with a C-terminal six-histidine tag for affinity purification. Agp1-FL represents the full-length protein. The covered range of amino acids is given at the right side of the panel; the first and last amino acids are abbreviated by the single-letter code and their position within the full-length sequence. The chromophore-binding Cys 20 is located at the N-terminal border of the PLD, as indicated by "C20" for Agp1-FL.

phytochromobilin, and most cyanobacterial phytochromes utilize phycocyanobilin; on the other hand, bacterial phytochromes from non-oxygenic photosynthetic and heterotrophic eubacteria and fungi incorporate biliverdin (BV) (*19*). In plant and most cyanobacterial phytochromes, the chromophore is bound to a Cys residue within the GAF domain. For *Agrobacterium* Agp1, BV was found to bind covalently to Cys 20 via its ring A vinyl side chain (*7*, *20*). This binding site is also used in all other BV-binding phytochromes that have been tested so far (*21*−*23*).

Phytochromes are synthesized in a "red-absorbing form" termed Pr which converts to a "far-red-absorbing form" termed Pfr upon light absorption. In darkness, the Pr form of most phytochromes is stable, whereas slow dark reversion from Pfr to Pr has been observed for many phytochromes, including Agp1 (*20*). The reverse dark reaction, i.e., dark conversion from Pr to Pfr, has been described for four bacterial phytochromes, including Agp2 (*3*, *8*, *21*, *24*). For Agp1 and Agp2, it has been shown by the use of locked chromophores that the chromophore stereochemistry is *ZZZssa* in the Pr form and *ZZEasa* or *EZEasa* in the Pfr form (*12*, *13*).

Electron microscopy measurements with plant phytochrome provided a low-resolution model in which two phytochrome holoprotein subunits form a Y-shaped molecule (*25*). Biochemical assays showed that the chromophore and the hinge region connecting the N-terminal sensory module with the C-terminal output module are more exposed in the Pfr form of plant phytochrome (*26*). The plant-specific double-PAS domain serves as nuclear localization signal and becomes exposed upon Pr to Pfr photoconversion (*27*). For cyanobacterial phytochrome Cph1, which dimerizes through its C-terminal histidine kinase (*28*, *29*), the N-terminal chromophore module without the histidine kinase has also been found to be able to form dimers and the subunit association has been found to be much stronger in the Pfr form than in the Pr form (*29*, *30*). This conformation-specific dimerization might be an important step in intramolecular signal transduction, but it is unclear whether the same mechanism holds for other phytochromes as well.

A crystal structure of the chromophore binding domain (CBD) of a bacterial phytochrome from *Deinococcus radiodurans* which entails the 321 N-terminal amino acids, including the GAF domain, has recently been published (*31*). These data showed that the GAF and PHY domains form an unusual knot which stabilizes the overall fold of the polypeptide. The amino acids of the chromophore pocket and those in the knot region are highly conserved among phytochromes (*31*). These findings together with biophysical measurements on different representatives of phytochromes (e.g., refs *11*, *32*, and *33*) suggest that the principal mechanisms behind photoconversion are evolutionarily conserved and identical in plant and bacterial phytochromes. Recent small-angle X-ray scattering measurements with the Pr form of the bacterial phytochrome BphP4 from *R. palustris* showed that this protein also has a Y-shaped structure which is formed by two subunits of the dimer (*34*). Despite the improved knowledge of phytochrome chromophore isomerization and protein structure, details about conformational changes that occur during photoconversion and lead to the modulation of histidine kinase activity and other signal transduction events are, however, only hardly understood.

In this study, we used Agp1 as a model phytochrome for protein conformational changes. The mobility of the Agp1 chromophore module on size exclusion chromatography increases upon Pr to Pfr photoconversion (*12*), which is reminiscent of the Cph1 light-dependent dimerization mentioned above. It is, however, unclear whether these mobility effects are based on differential protein shapes or conformation-dependent dimerization as in Cph1. Therefore, the quaternary structure was also probed by protein cross-linking, a method which has previously been utilized in one study with plant phytochromes (*35*). We also analyzed protein conformational changes by limited proteolysis, which allowed us to test for conformational changes that are independent of dimerization. By using fragments that cover different domains of Agp1, we were able to gain an insight into the topography of these domains with respect to Pfr formation and subunit interaction.

EXPERIMENTAL PROCEDURES

Agp1 Expression Vectors. All expression vectors encode proteins with a C-terminal polyhistidine tag for Ni^{2+} affinity purification. Expression clones for full-length Agp1 and for six different deletion proteins as summarized in Figure 1 were used. The pAG1 expression vector for the full-length protein, termed Agp1-FL here, and the vector pAG1-M15, which encodes the Agp1-M15 protein, have been described previously (*14*, *36*). Agp1-M15 consists of the 504 N-terminal amino acids of Agp1 and contains the PLD, the GAF domain, and the PHY domain but lacks the C-terminal histidine kinase module (Figure 1). For other truncation constructs, the pAG1 or pAG1-M15 plasmids were used as a template for PCR-based deletion mutagenesis.

For the construction of pAG1-M16 (protein, Agp1-M16), the sequence for the 15 C-terminal amino acids of Agp1-M15 (Leu 490−Asp 504) were removed using the primer pair st2 (CTCCCTCGCTGCCGCAAGTTCG)/ti12 (CATCACCATCACCATCACTAAGCTTAATTAG). For the construction of pAG1-M17 (protein, Agp1-M17), the sequence for the 23 C-terminal amino acids of Agp1-M15 (Pro 482−Glu 504) was removed using the primer pair st3 (CTCTGACACGGGAAAGGAGG)/ti12. For the construction of

pAG1-M20 (protein, Agp1-M20), the sequence for the PHY domain (amino acids Asp 314−Glu 504) was removed using the primer pair t17 (CTGGGAACTCTGCTCCATCG)/ti12. For the construction of pAG1-M15Δ9N (protein, Agp1-M15Δ9N), the region that encodes nine N-terminal amino acids (Gln 2−Met 10) was deleted by using the primer pair nm-cut-as (CATAGTTAATTTCTCCTCTTTAATGAATTCTG)/nm-cut-se (AGTTCACATACGCCGAAACTGGATAGTTGC). For pAG1-M15Δ18N (protein, Agp1-M15Δ18N), the region which encodes 18 N-terminal amino acids (Gln 2−Ser 19) was deleted using the primer pair nm-cut as/t18 (TGCGGCGCAGAGCCCATCCAC). The Met start codon was retained in all cases.

The PCR profile was as follows: 95 °C for 1 min and, 24 times, 95 °C for 30 s, 60 °C for 1 min, and 72 °C for 11 min. The original template plasmid was digested with DpnI. After agarose gel purification and phosphorylation with T4 kinase, the PCR products were self-ligated with T4 Ligase (NEB, Beverly, MA) and cloned in *Escherichia coli* XL1-Blue cells (Stratagene). Positive clones were identified by protein expression (*20*). All constructs were confirmed by DNA sequencing.

Protein Expression and Purification. All proteins used in this study were purified as apoproteins without a chromophore. Cell culture, protein extraction, and Ni^{2+} affinity purification were performed as described for the full-length protein (*36*). The eluate of Ni affinity chromatography was concentrated by ammonium sulfate precipitation and suspended in "basic buffer" [50 mM Tris-HCl, 5 mM EDTA, and 300 mM NaCl (pH 7.8)]. The protein concentration was estimated from the absorbance at 280 nm. The extinction coefficient ϵ_{280} was obtained from the integrated ϵ_{280} values of absorbing amino acids as given by the Vector NTI program. Purified proteins were stored at −80 °C.

Assembly, Photoconversion, and Dark Reversion. All spectral assays were performed at 18 °C. Assembly kinetics was measured as described previously (*12*). The protein was diluted to obtain an A_{280} of ∼1. The final concentration of BV was 5 μM. The spectra were normalized to A_{280}. For size exclusion chromatography, limited proteolysis, and cross-linking studies, the BV chromophore was used at an excess molar concentration (10−15 μM protein and 20 μM BV). For photoconversion, the sample was irradiated for 5 min with red light from a 655 nm light-emitting diode (50 μmol m^{-2} s^{-1}). For dark reversion, the absorbance of the (dark-adapted) adduct was measured at 750 nm. This value was taken to be 0% photoproduct. Thereafter, the sample was photoconverted via saturating red light irradiation. After the light had been switched off, the absorbance at 750 nm was measured continuously for ≥100 min using the "time drive" program of the photometer. The absorbance value after the light had been switched off is taken to be 100% photoproduct. The percent photoproduct values are presented in Figure 4. The same data were fitted to an exponential decay function with two components using the nonlinearized least-squares fitter of Microcal Origin (version 5).

Analytical Size Exclusion Chromatography. For size exclusion chromatography (SEC), a Superdex 200 HR 10/30 column (Amersham/Pharmacia, Freiburg, Germany) was used as described previously (*12*). The elution buffer was 50 mM Tris-HCl, 150 mM NaCl, and 5 mM EDTA (pH 7.8). The system was calibrated with marker proteins cytochrome *c* (12.4 kDa), carbonic anhydrase (29 kDa), bovine serum albumin (66 kDa), alcohol dehydrogenase (150 kDa), β-amylase (299 kDa), apoferritin (443 kDa), and blue dextran (2000 kDa) (Sigma).

Limited Proteolysis and Electrophoresis. Agp1 was digested with trypsin (TPCK-treated; Sigma-Aldrich) or endoproteinase Glu-C (V8) at 18 °C. The final protease concentrations were 0.6 and 10 μg/mL, respectively, and the incubation times were 30 min and 3 h, respectively. The concentration of the Agp1 protein varied as given in the figure legends. In general, proteolysis was performed in darkness, but the incubation of the photoproduct was performed under continuous irradiation with red light (655 nm, 32 μmol m^{-2} s^{-1}). In this case, the protease was added 10 min after the onset of light. We estimated that under these irradiation conditions, the fraction of phytochrome molecules in an intermediate stage is <0.3% (see refs *11*, *20*, and *37* for formulas and parameters). Proteolysis was stopped by the addition of SDS sample buffer [from a stock solution to achieve final concentrations of 10% glycerol, 2% SDS, 100 mM 1,4-dithio-DL-threitol, 0.003% bromophenol blue, 80 mM Tris-HCl (pH 6.8)]. After being heated to 100 °C for 5 min, the polypeptides were subjected to NuPage gel electrophoresis (Invitrogen) using 4 to 14% gradient gels and MES running buffer according to the manufacturer's instructions. Although the gel system contains lithium dodecyl sulfate as a detergent, we use the common abbreviation SDS−PAGE for protein electrophoresis throughout this work. Note that (in contrast to the protocol of the manufacturer) a SDS buffer was used for the preparation of protein samples. Chromopeptides were detected by the Zn^{2+}-induced fluorescence (*29*, *38*), and the peptides were stained with Coomassie.

HPLC and Mass Spectrometry. After peptide electrophoresis and Coomassie staining, the acryl amide gels were washed twice for 1 h in 500 mL of water. Gel slices containing the peptides of interest were cut out. The gel pieces were washed in a 200 mM NH_4HCO_3/50% acetonitrile solution and dried in a SpeedVac. The gels were rehydrated in a 20 μg/mL trypsin solution (Promega, Madison, WI) and incubated for 16 h at 37 °C. Peptides were extracted from the gel slices by diffusion in water. The peptides were identified by liquid chromatography and mass spectrometry (LC−MS/MS) using an UltimateTM nano HPLC system (LC Packings, Amsterdam, The Netherlands) and a Qstar Pulsar mass spectrometer (Applied Biosystems, Foster City, CA). The MS data were analyzed using the Mascot protein identification software (Matrix Science, London, U.K.).

Cross-Linking Studies. For cross-linking of interacting peptides, glutaraldehyde (Sigma) was used. The final protein concentrations were 1, 0.5, 0.25, 0.13, 0.06, and 0.03 mg/mL, and the final glutaraldehyde concentration was always 5 mM. Proteins and cross-linker were diluted with potassium phosphate buffer [20 mM Na_2HPO_4/NaH_2PO_4 (pH 7.8)], mixed, and incubated at 18 °C for 3 h. For cross-linking of photoconversion products, the samples were irradiated continuously as described above for the protease treatment. The cross-linker was added 10 min after onset of red light. In some cases, cross-linking was performed with bis-(sulfosuccinimidyl)suberate (Sigma). In this case, the cross-linker concentration was varied between 1.5 and 15 mM.

The cross-linking reactions were stopped with SDS sample buffer and the solutions subjected to NuPage (Invitrogen) gel electrophoresis. Peptide bands were stained with Coomassie. Cross-linked samples were also subjected to SEC. In some cases, 0.5 mL fractions were collected and subjected to NuPage gel electrophoresis as described above.

RESULTS

Recombinant Agrobacterium Phytochrome Constructs. In this work, we have used recombinant, His-tagged, full-length *Agrobacterium* phytochrome Agp1, termed Agp1-FL here, and various deletion constructs, which are summarized in Figure 1. Agp1-M15 contains all domains of the photosensory module with the PLD, the GAF domain, and the PHY domain but lacks the C-terminal histidine kinase (*14*). In Agp1-M16 and Agp1-M17, the C-terminus of Agp1-M15 was truncated by 15 and 23 amino acids, respectively. Agp1-M20 contains the 313 N-terminal amino acids, including the PLD and the GAF domain, but lacks the PHY domain. This fragment is comparable with the chromophore binding domain of *Deinococcus* phytochrome DrBphP which has been used for the determination of a crystal structure (*31*). We also constructed fragments in which N-terminal amino acids are missing. The constructs Agp1-M15Δ9N and Agp1-M15Δ18N are derived from Agp1-M15 but lack amino acids 2−10 and 2−19, respectively. All proteins were readily expressed in *E. coli*, but the level of expression and the solubility of the proteins differed. The highest yields were obtained for Agp1-FL and Agp1-M15. Agp1-M15Δ18N was only weakly expressed (∼5% of the full-length protein). The yields of Agp1-M16 and Agp1-M17 were ∼80−90% of that of Agp1-FL, but the solubility of both proteins in the crude extract was very low. The yields of Agp1-M20 and Agp1-M15Δ9N were 60−70 and 40−50% of that of Agp1-FL, respectively. The solubility of Agp1-M20 was rather low, but the solubility of Agp1-M15Δ9N was comparable with that of Agp1-M15.

Chromophore Assembly. The autocatalytic incorporation of the chromophore, chromophore assembly, is accompanied by an absorbance increase in the wavelength region of the Q-band (the long wavelength absorption around 700 nm) and other characteristic spectral changes. We followed the assembly of all fragments by recording UV−vis spectra in 5 min intervals after the apoproteins were mixed with BV. The assembly spectra of Agp1-FL, Agp1-M15, Agp1-M15Δ18N, and Agp1-M15Δ9N were comparable with each other. In those cases, the assembly was completed between 1 and 5 min after the chromophore and protein were mixed (see Figure 2a for Agp1-FL). The spectra obtained during the Agp1-M16 and Agp1-M17 assembly were also similar to each other but different from that of Agp1-FL (see Figure 2b for Agp1-M16). When BV and protein were mixed, the absorbance at 700 nm increased only slightly. Zn^{2+}-induced fluorescence (*38*) that was performed with Agp1-M16 after the assembly showed that the chromophore was covalently bound to the protein (data not shown). Chromophore incorporation seems thus not to be affected in Agp1-M16 and Agp1-M17, but the Q-band extinction coefficient of the adducts is significantly lower than that of all other constructs used in this study. Both Agp1-M16 and Agp1-M17 seem to be improperly folded. In crude extracts, the major portion of these proteins was insoluble (see above). The purified,

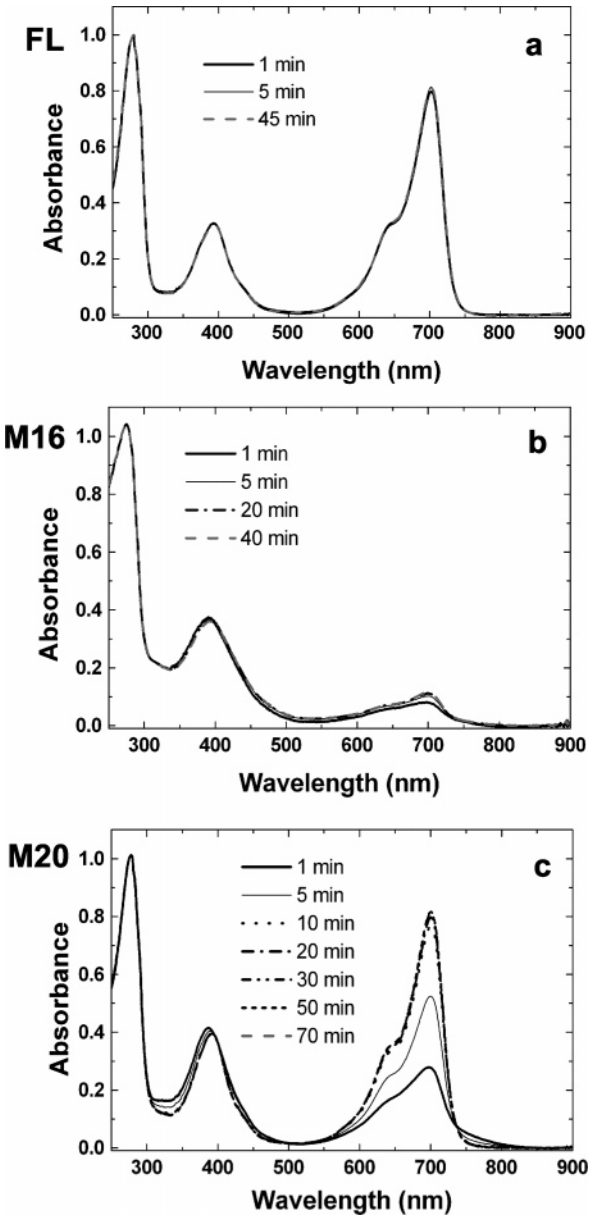

FIGURE 2: Spectral changes during assembly of Agp1 constructs with BV: (a) Agp1-FL, (b) Agp1-M16, and (c) Agp1-M20. The patterns of Agp1-M15, Agp1-M15Δ9N, and Agp1-M15Δ18N were very similar to that of Agp1-FL. The pattern of Agp1-M17 was very similar to that of Agp1-M16.

soluble proteins revealed several peaks on SEC in the high-molecular mass range (data not shown), which is interpreted as an indication of protein aggregation. Therefore, these proteins were not further analyzed. Agp1-M20 assembly was rather slow and completed ∼60 min after mixing (Figure 2c). Our assembly studies show that the removal of amino acids 2−19 does not affect chromophore incorporation, whereas the removal of the PHY domain has a negative impact on chromophore assembly.

Comparison of Adduct and Photoproduct Spectra. Agp1-FL, Agp1-M15, and Agp1-M15Δ9N adduct spectra were indistinguishable before and after photoconversion (see Figure 3a for Agp1-FL). Photoconversion of these adducts is characterized by a shift of the Q-band from 702 to 750 nm and a shift of the Soret band (absorption maximum in the blue spectral region) from 400 to 415 nm. The Agp1-M20 adduct spectrum (Figure 3b) resembles that of the above

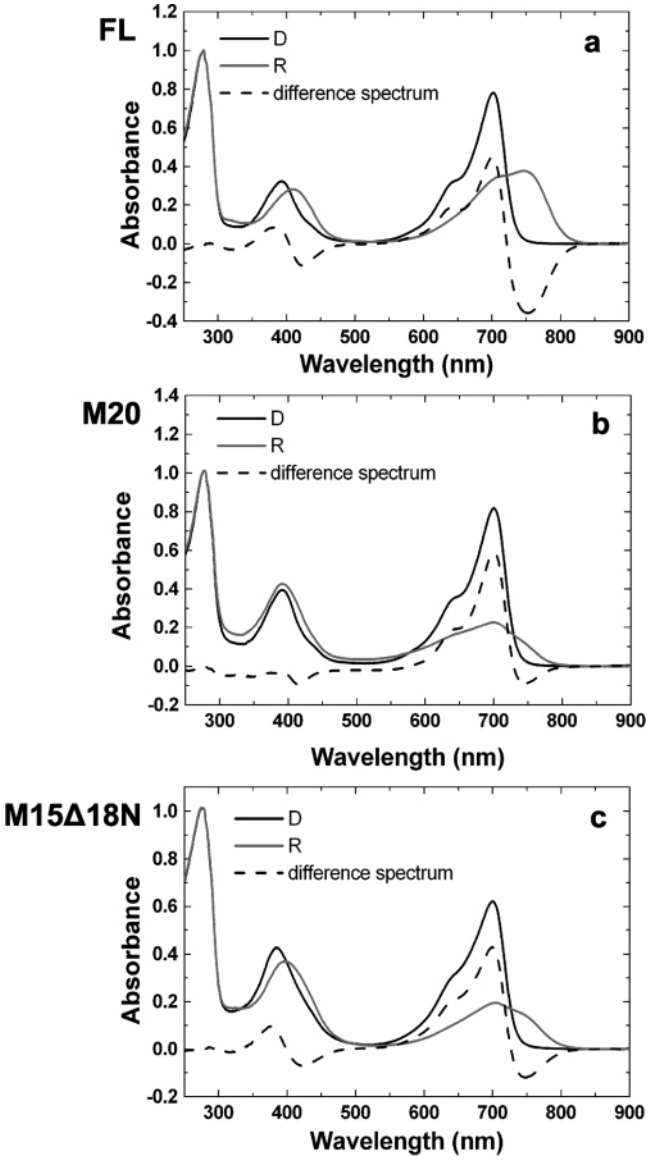

FIGURE 3: Spectra of Agp1-FL (a), Agp1-M20 (b), and Agp1-M15Δ18N (c) adducts after dark incubation (black lines) and saturating red irradiation (gray lines). The differences between both spectra are given as the dashed lines. Spectra of Agp1-M15 and Agp1-M15Δ9N were comparable with that of Agp1-FL.

adducts. Photoconversion resulted also in a red shift of the Q-band, but the absorption decrease in that spectral region was more pronounced than in the case of the other adducts. Moreover, the position of the Soret band did not change, and the absorption in that spectral region increased. The spectral properties of the photoproduct are similar to those of the CBD of *Deinococcus* phytochrome (*31*), the N-terminal 450-amino acid fragment of *Arabidopsis* phytochrome B (*39*), and a 39 kDa proteolytic fragment of oat phytochrome (*40*, *41*). A cryotrapped photocycle intermediate of Agp1, meta-Rc, also has similar spectral properties (*11*). The Agp1-M15Δ18N adduct is also spectrally similar to the Pr form of the full-length adduct (Figure 3c). The photoproduct spectrum of this adduct is comparable with that of Agp1-M20 in the Q-band region but similar to the photoproduct of Agp1-FL in the Soret band region.

Dark Reversion. Like many other phytochromes, Agp1 converts slowly from Pfr to Pr in darkness (*20*). We monitored the dark reversion of the different adducts by measuring the absorbance at 750 nm after photoconversion (Figure 4). The curves fitted well to an exponential decay function with either one (for Agp1-M20) or two (for other chromopeptides) components (Table 1). Dark reversion of Agp1-M15 (time constants, $t_1 = 23$ min, and $t_2 = 160$ min) was slower than that of the full-length adduct ($t_1 = 7$ min, and $t_2 = 150$ min), showing that the histidine kinase module has a negative impact on the dark stability of Pfr. Dark reversion of Agp1-M15Δ9N ($t_1 = 18$ min, and $t_2 = 150$ min) was faster than that of Agp1-M15 but still slower than that of the full-length protein. Thus, the nine N-terminal amino acids have a positive impact on the dark stability of Pfr. Dark reversion of Agp1-M15Δ18N appears to be very fast, because the fast component has a rather high amplitude of 72%. The time constant of the fast component ($t_1 = 10$ min) is in the range of that the wild-type protein. Therefore, amino acids 10−19 seem to be important for the stabilization of the second phase of dark reversion. The fast component was missing in Agp1-M20, which therefore has a rather slow dark reversion. It should be noted that the truncation of the PHY domain in *Arabidopsis* phytochrome B had the opposite effect on the dark reversion (*39*).

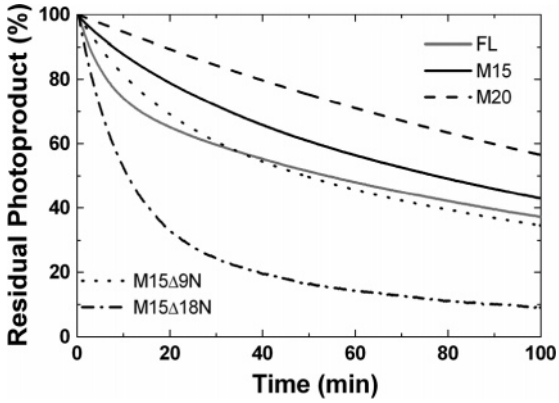

FIGURE 4: Dark reversion of Agp1-FL (gray solid line), Agp1-M15 (black solid line), Agp1-M20 (dashed line), Agp1-M15Δ9N (dotted line), and Agp1-M15Δ18N (dashed−dotted line). After photoconversion by saturating red irradiation of the BV adducts, the absorption at 700 nm (as a value for Pr) was measured. The "residual photoproduct" is calculated by $[1 - (A_t - A_R)/(A_D - A_R)] \times 100\%$, where A_D is the absorption after dark assembly, A_R is the absorption after saturating red irradiation, and A_t is the absorption at time t. The value of 100% is equivalent to the amount of photoproduct directly after irradiation.

Table 1: Amplitudes (A_1 and A_2) and Time Constants (t_1 and t_2) of Dark Reversion Given in Figure 4[a]

	A_1 (%)	t_1 (min)	A_2 (%)	t_2 (min)
Agp1-FL	28	7	72	150
Agp1-M15	19	23	81	160
Agp1-M20	100	175	−	−
Agp1-M15Δ9N	35	18	65	150
Agp1-M15Δ18N	72	10	30	80

[a] The data were fitted to an exponential decay function with two components. The fit of the Agp1-M20 data required one component only.

Size Exclusion Chromatography. We compared apoprotein, nonirradiated, and photoconverted BV adducts of the different constructs by size exclusion chromatography (SEC). There was no mobility difference between the nonirradiated Agp1-FL adduct and the photoconverted holoprotein. The elution profile of the apoprotein was also not significantly

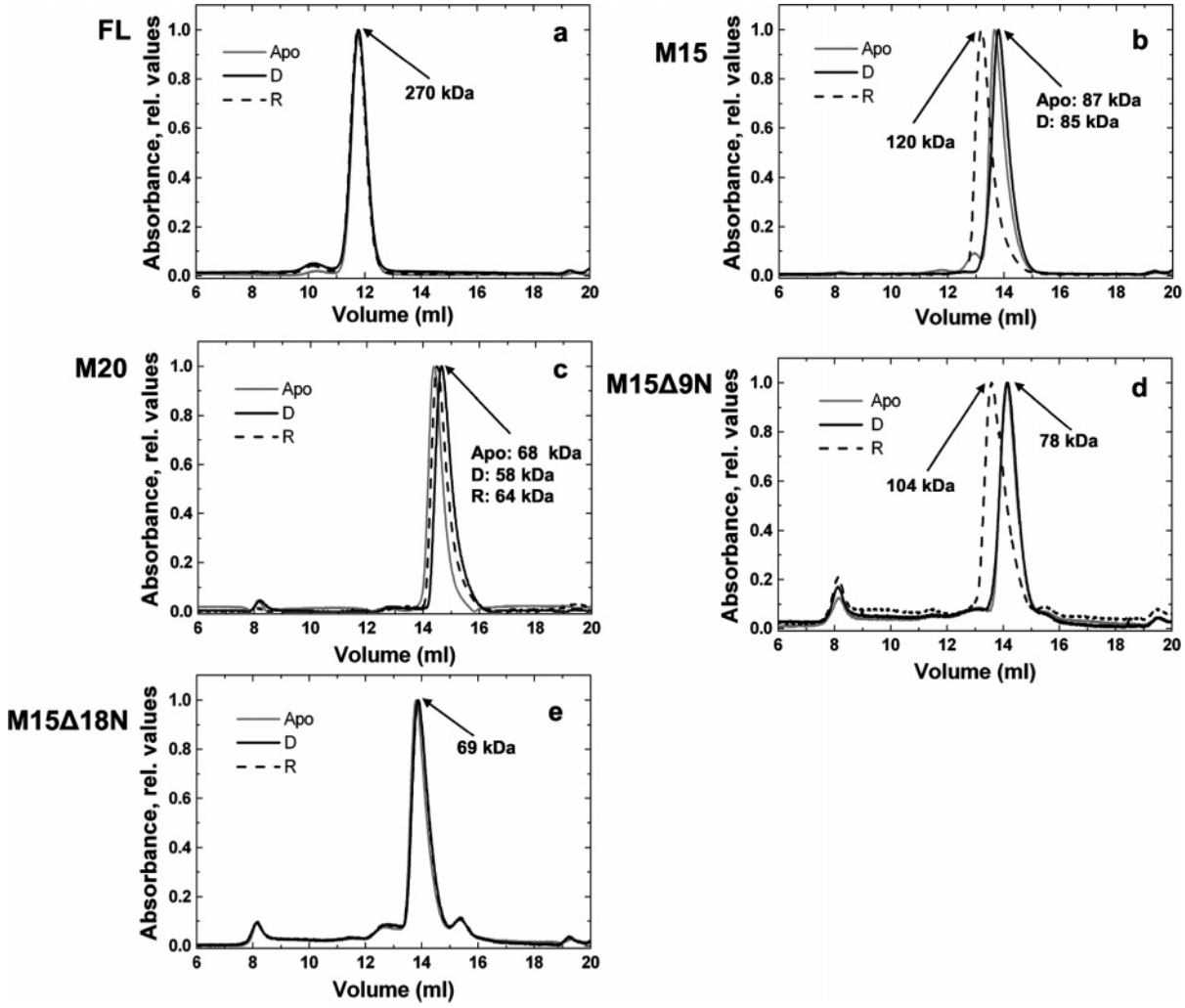

FIGURE 5: Size exclusion chromatography with Agp1-FL (a), Agp1-M15 (b), Agp1-M20 (c), Agp1-M15Δ9N (d), and Agp1-M15Δ18N (e). The profiles of the apoproteins (Apo), the nonirradiated adducts (D), and the irradiated adducts (R) are depicted by the solid gray, solid black, and dashed black lines, respectively. The elution profiles were normalized to the highest value.

different from those of the holoproteins. The apparent molecular mass was around 270 kDa (Figure 5a). For Agp1-M15, however, we observed significant mobility differences among the apoprotein, the nonirradiated adduct (Pr), and the irradiated adduct (high Pfr level). The apparent molecular masses were 87, 85, and 120 kDa, respectively (Figure 5b). The results for Agp1-M15Δ9N (Figure 5d) were comparable with those for Agp1-M15, except that the apoprotein and the nonirradiated adduct did not differ significantly. The apparent molecular size of the apoprotein and the nonirradiated adduct was 78 kDa and that of the irradiated adduct 104 kDa.

The light-induced change in SEC mobility was lost in Agp1-M15Δ18N (Figure 5e). Both the nonirradiated and irradiated adducts migrated with an apparent molecular mass of 69 kDa. It should be noted that the fast dark reversion of Agp1-M15Δ18N (Figure 4) might extinguish a possible light effect on the mobility of the adduct. The elution profile of the apoprotein was indistinguishable from that of the BV adducts. With Agp1-M20, we obtained subtle differences between the nonirradiated and irradiated adduct and the apoprotein (Figure 5c). The apparent molecular masses were 58, 64, and 68 kDa, respectively.

Protein Cross-Linking. Size exclusion chromatography can be regarded as an assay for quaternary structure. Comparing the apparent molecular mass in the native state with the calculated molecular mass of the monomer can give an idea about the numbers of subunits that are bound together. However, these SEC data were not conclusive in this respect. For example, the apparent molecular mass of the full-length protein of 270 kDa could be explained in several ways. This value could relate to the dimer of Agp1, which has a molecular mass of 2 × 85 kDa (170 kDa), and a nonglobular shape of the protein could increase its mobility via SEC. Alternatively, four Agp1 subunits might be bound together, and the mobility could be reduced by an interaction with the gel matrix. Another restriction of SEC is that the proteins are diluted during separation in an unpredictable manner and that weakly interacting subunits will dissociate during the analysis. The Agp1-M15 SEC results point to a Pfr-dependent dimerization, but these data also demand an independent approach. For these reasons, we tested the quaternary structure of Agp1 constructs also by protein cross-linking.

For most cross-linking experiments, glutaraldehyde was used at a final concentration of 5 mM. When the nonirradiated Agp1-FL adduct was treated with glutaraldehyde under standardized conditions, the holoprotein was still photoactive. The UV−vis spectrum of the nonirradiated sample was comparable with that of the nontreated control, but the

spectrum of the photoproduct resembled closely that of Agp1-M20: irradiation resulted in a red shift of the Q-band and a decrease in absorbance, whereas the position of the Soret band was not affected during photoconversion (data not shown). For these reasons, cross-linking data do probably not exactly reflect the features of the native proteins. Most conclusions that are drawn from cross-linking results are, however, independent of the spectral form of the Agp1 constructs. As far as differences between Pr and Pfr are concerned, we assume that the results reflect at least qualitatively the situation of the nontreated photoproduct: the cross-linker was always added after the completion of photoconversion. The combination of cross-linking and SEC presented below supports this assumption.

To be able to distinguish between strong and weak interactions, we always performed cross-linking at different protein concentrations between 0.03 and 1 mg/mL. If an interaction is strong, cross-linked dimers or oligomers will be formed at any concentration; if the interaction is weak, cross-linked products will be formed at high concentrations only. To compensate for dark reversion, the irradiated adducts were kept under constant illumination throughout the glutaraldehyde incubation.

The monomer of the untreated full-length protein migrates with an apparent molecular mass of 85 kDa on SDS−PAGE. For all protein concentrations, a cross-linked dimer, which migrates with an apparent molecular mass of 162 kDa on SDS−PAGE, was formed. For protein concentrations of ≥0.25 mg/mL, an oligomer which has an apparent molecular mass of more than 300 kDa was also detected. With 1 and 0.5 mg/mL protein, even larger oligomers were formed. The monomer band was absent in all glutaraldehyde-treated samples (Figure 6a). We found no difference between the three different forms, apoprotein, nonirradiated adduct, and irradiated adduct. The cross-linking data confirmed the assumption that Agp1 forms stable dimers and show also that more than two subunits, probably multitudes of two, can bind to each other. Concluding from the dilution series, we assume that the dissociation constant for the dimerization of full-length Agp1 is far below 0.03 mg/mL, i.e., ∼0.3 μM, and that the dissociation constant for oligomer formation is in the range of 0.5 mg/mL, i.e., ∼5 μM.

The non-cross-linked Agp1-M15 monomer migrates with an apparent molecular mass of 55 kDa on SDS−PAGE. After treatment with glutaraldehyde, the monomer band was still present, but additional bands of 50, 110, 147, and 193 kDa appeared (Figure 6b). The same cross-linking products were also obtained with bis(sulfosuccinimidyl)suberate, a homobifunctional cross-linker which reacts with lysine side chains and has a spacer arm length of 11 Å (data not shown). We assume that the 50 kDa band results from an intramolecular cross-linking within one monomer subunit. The crystal structure of the CBD of DrBphP showed that this phytochrome protein forms a knot (*31*). The 50 kDa band could correspond to a monomer in which the knot is stabilized by the cross-linker and therefore not untied by the SDS treatment. The 110, 147, and 193 kDa bands are assigned to the dimer, trimer, and tetramer, respectively. The dimer band and the 50 kDa band were obtained with all tested protein concentrations, whereas trimer and tetramer bands were obtained with higher protein concentrations only. For protein concentrations between 0.03 and 0.13 mg/mL, the dimer band of the irradiated adduct (high Pfr level) was stronger than the corresponding band of the apoprotein or the nonirradiated adduct (Pr only). This suggests that the dimerization is stronger in the Pfr form than in both other forms. This is in accordance with cyanobacterial phytochrome Cph1 (*29*, *30*) and explains the Pr versus Pfr mobility difference found for the Agp1-M15 adduct in our SEC experiments (Figure 5b).

The dimer formation pattern of Agp1-M15Δ9N (Figure 6d) was similar to that of Agp1-M15 (Figure 6b). An intramolecular cross-link was also formed, as indicated by the appearance of the 50 kDa band. There were, however, no cross-linked oligomers, showing that the nine N-terminal amino acids mediate oligomer formation in Agp1-M15.

With Agp1-M15Δ18N, cross-linked dimers were also found for all protein concentrations that were tested. At lower concentrations (0.03−0.25 mg/mL), the dimer band of the irradiated adduct was slightly stronger than the dimer band of the nonirradiated adduct or the apoprotein (Figure 6e). Therefore, the extent of dimer formation of this adduct is also increased upon photoconversion. The fact that this light effect is not seen in the SEC experiments might be due to the rather fast dark reversion. As expected, Agp1-M15Δ18N formed no cross-linked oligomers. Quite interestingly, the intramolecular cross-link was also missing. Thus, an amino acid between positions 10 and 19 is involved in the intramolecular cross-linking reaction. The only lysine residue in this region is Lys 16.

After cross-linking of Agp1-M20, monomers, dimers, trimers, and tetramers with molecular masses of 33, 75, 112, and 151 kDa were found (Figure 6c). The dimer band was always the strongest band in the Agp1-M20 assays. We found no significant difference among the apoprotein, the nonirradiated adduct, and the irradiated adduct with respect to dimer formation. There was no indication of an intramolecular cross-link in Agp1-M20 either.

Combination of SEC and Protein Cross-Linking. Size exclusion chromatography of cross-linked proteins allows a better assignment of the SEC elution peaks. When the Agp1-FL adduct was cross-linked in the nonirradiated or irradiated state, the protein eluted from the SEC column with two peaks that correspond to molecular sizes of ∼620 or 660 kDa and 260 or 270 kDa (Figure 7a,b). The 260 or 270 kDa peak is in accordance with the 270 kDa peak of the untreated sample. The fractions under the 260 or 270 kDa SEC peaks contain only covalent dimers, as shown by subsequent SDS−PAGE. The peak is thereby defined as a dimer peak. Thus, the major fraction of full-length Agp1 migrates as a dimer on SEC, irrespective of whether the protein is cross-linked. The fractions under the 620 or 660 kDa SEC peaks contained cross-linked dimers and oligomers with more than two subunits. Since this SEC peak height is drastically increased by cross-linking, the oligomers of non-cross-linked Agp1 must dissociate during column separation. These data confirm the findings given above about the weak association of two or more dimers within an oligomer. We did not test for the significance of the differences that were found between cross-linked nonirradiated and cross-linked irradiated adducts.

When the nonirradiated Agp1-M15 adduct was cross-linked and subjected to SEC, three peaks with apparent molecular masses of 340, 140, and 80 kDa were resolved (Figure 7c). SDS−PAGE showed that the fractions under

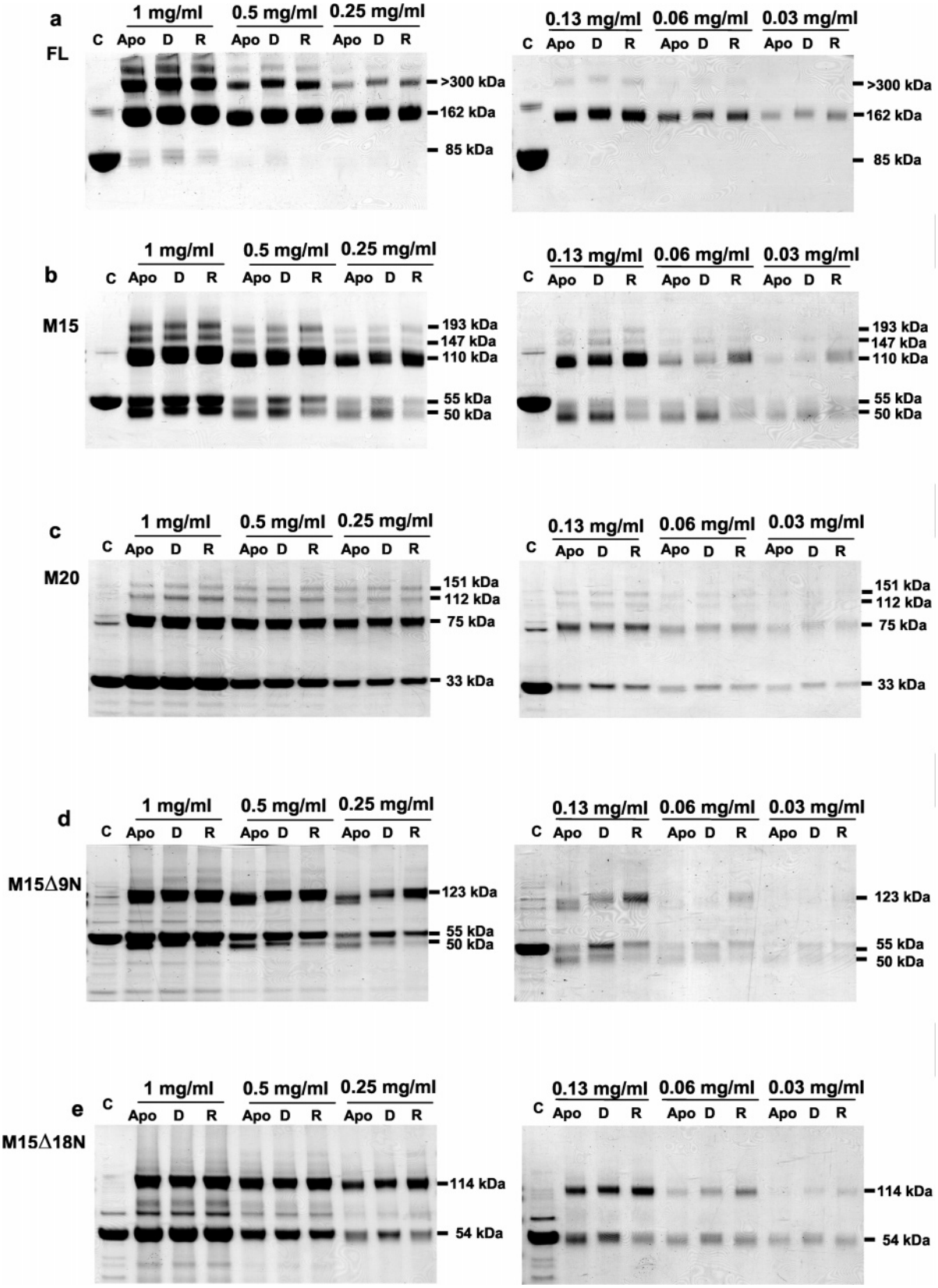

FIGURE 6: Cross-linking experiments with Agp1-FL (a), Agp1-M15 (b), Agp1-M20 (c), Agp1-M15Δ9N (d), and Agp1-M15Δ18N (e) treated with glutaraldehyde and subjected to SDS−PAGE. The protein concentrations are given above each panel. C denotes the untreated control (monomer), Apo the cross-linked apoprotein, D the cross-linked nonirradiated adduct, and R the cross-linked photoconverted adduct. The latter samples were continuously irradiated during the glutaraldehyde incubation. The molecular sizes as judged from marker proteins are given at the right side of each subpanel.

the 80 kDa peak contained the non-cross-linked monomer and the product with the intramolecular cross-link. The 140 kDa SEC peak contained both monomeric forms but also the cross-linked dimer, which appeared here with two separate bands around 110 kDa on SDS−PAGE. The difference between these bands is most likely related to the

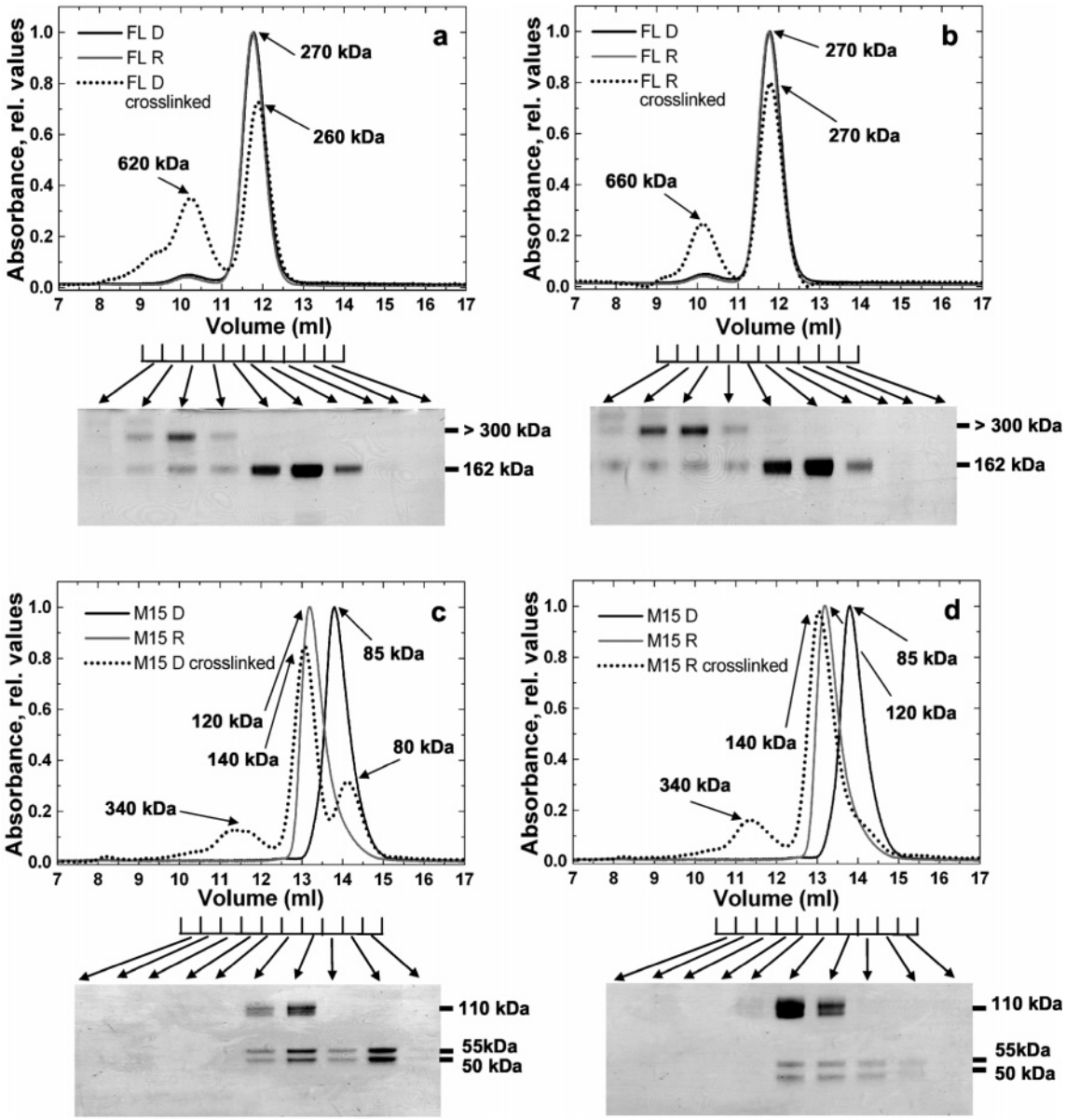

FIGURE 7: Combination of cross-linking and SEC. (a) The nonirradiated adduct of Agp1-FL was cross-linked and subjected to SEC. The elution profile is given in the top panel (dotted line), together with the elution profiles of non-cross-linked adducts (black solid line for the nonirradiated adduct and gray line for the irradiated adduct of Agp1-FL). Fractions (0.5 mL) were subjected to SDS−PAGE (bottom panel), and the allocation of each fraction to the elution profile is indicated by bars and arrows that are drawn beneath the top panel. (b) Like panel a, except that the irradiated adduct of Agp1-FL was subjected to SEC (dotted line). (c) The nonirradiated adduct of Agp1-M15 was cross-linked and subjected to SEC and SDS−PAGE as described for panel a. The elution profiles of the cross-linked adduct (dotted line) are shown in comparison with the elution profiles of non-cross-linked adducts (black solid line for the nonirradiated adduct and gray line for the irradiated adduct of Agp1-M15). Data are presented as in panel a. (d) Like panel c, except that the irradiated adduct of Agp1-M15 was subjected to SEC (dotted line).

intramolecular cross-link. The 140 kDa SEC peak thus corresponds to a native dimer, in which cross-linked dimers and non-cross-linked dimers migrate together. The proteins of the 340 kDa SEC peak fractions were below the detection limit of SDS−PAGE. When the Agp1-M15 adduct was cross-linked in the irradiated form and subjected to SEC, two peaks with apparent molecular masses of 340 and 140 kDa were resolved (Figure 7d). The 140 kDa peak again contains cross-linked dimers. The SEC comparison between cross-linked and non-cross-linked irradiated Agp1-M15 adducts shows again that the non-cross-linked species elutes predominately as a dimer.

Limited Proteolysis. Conformational changes of proteins can be probed by limited proteolysis, a method which has been applied in the study of plant and cyanobacterial phytochromes (*29*, *42*). In this study, we subjected Agp1 constructs to endoproteinase GluC (V8) and separated the cleavage products by SDS−PAGE. Since the chromophore attachment site Cys 20 is close to the N-terminus, the presence or absence of the chromophore gives further information about the position of the cleavage site(s). If the chromophore is present, the SDS−PAGE mobility of the fragment in comparison with that of known fragments allows assignment of the position of the C-terminal cleavage site within a range of ~30 amino acids. Therefore, chromophore-bearing peptides were detected by Zn^{2+} fluorescence (*38*) before the gels were stained with Coomassie for visualization of all peptide bands.

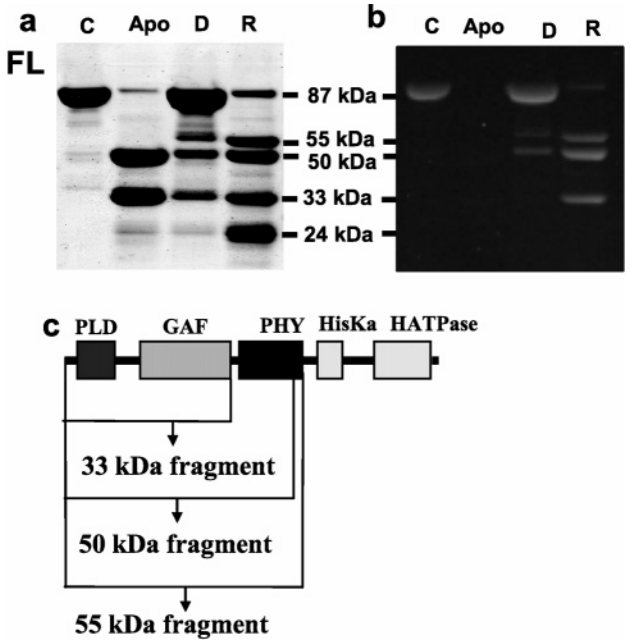

FIGURE 8: Proteolysis of Agp1-FL with V8. (a) Coomassie stain and (b) Zn^{2+}-induced fluorescence of a SDS−PAGE gel. The apoprotein (Apo), the nonirradiated adduct (D), and the irradiated adduct (R) were incubated with V8 and the samples subjected to SDS−PAGE along with the untreated control (C). The apparent molecular sizes of the fragments as judged from marker proteins are given between both panels. (c) Proposed cleavage sites of the 55, 50, and 33 kDa fragments.

When the full-length protein was subjected to V8 proteolysis, fragments of 55, 50, 33, and 24 kDa were obtained. The cleavage patterns of apoprotein, the nonirradiated adduct, and the irradiated adduct were significantly different: digested apoprotein contains only 50 and 33 kDa fragments. A large portion of the nonirradiated adduct remained virtually undigested; in addition, 55, 50, and 33 kDa fragments were present. The digest with the irradiated adduct contained all four fragments and some apparently undigested protein (Figure 8a,b).

The predicted V8 cleavage sites are summarized in Figure 8c. The 55 kDa fragments are comparable with Agp1-M15, since they contain the chromophore and run with the same mobility on SDS−PAGE. Mass spectrometry analyses imply that the C-terminal amino acid of the 55 kDa fragment is Glu 501, which is located at the C-terminus of the PHY domain, i.e., close to the hinge region between the chromophore module and the histidine kinase. The exact cleavage site could not be determined by mass spectrometry and might as well be located several amino acids toward the C-terminal side of Glu 501. The differential cleavage pattern shows that the hinge region of Agp1 becomes exposed upon photoconversion from Pr to Pfr. The 50 and 33 kDa fragments that arose in Agp1-FL and Agp1-M15 digests also contain the chromophore. We predict that the cleavage site of the 50 kDa fragment lies in the C-terminal portion of the PHY domain. The cleavage site of the 33 kDa fragment lies in the transition from the GAF domain to the PHY domain, since this fragment has the same mobility on SDS−PAGE as Agp1-M20. The 24 kDa fragment of the digest with the irradiated adduct contains no chromophore and must bear at least a part of the histidine kinase, since it is missing in the Agp1-M15 digests (see below).

The Agp1-M15 apoprotein was digested to a 50 kDa fragment and to a smaller extent to a 33 kDa fragment. When proteolysis was performed with the nonirradiated adduct, a small fraction of the protein was digested to a 50 kDa fragment but the major fraction appeared to be undigested. The digest with the irradiated adduct yielded a 50 kDa fragment and a 33 kDa fragment (Figure 9a,b). The cleavage sites are most likely identical with those of the corresponding fragments that arose during Agp1-FL digestion.

The Agp1-M15Δ18N V8 digestion pattern was comparable to that of Agp1-M15, but the digest with the irradiated adduct was more pronounced than in Agp1-M15 (Figure 9c). We therefore propose that the 19 N-terminal amino acids protect this cleavage site. Agp1-M20 seems to be unaffected by the V8 protease (Figure 9d).

DISCUSSION

Phytochrome photoconversion is an event which triggers a broad number of developmental processes in plants, bacteria, and fungi. Many bacterial phytochromes, including *Agrobacterium* Agp1, are light-regulated histidine kinases, and the study of light-induced conformational changes might provide insight into general mechanisms behind the modulation of histidine kinase activity. Our studies will also provide insight into phytochrome assembly and photoconversion, processes which are probably similar in all phytochromes. By using different truncation fragments of Agp1, we were able to define functions of protein regions with respect to spectral properties and quaternary structure.

Dimer Formation, the Role of the Histidine Kinase, and the N-Terminal Part of the Protein. As in other sensory proteins, the histidine kinase module mediates strong protein dimerization of Agp1. The full-length protein forms stable dimers down to the lowest concentrations that were tested (0.3 μM, Figure 6a). If the histidine kinase module is lacking, the extent of subunit interaction is significantly reduced. In Agp1-M15, Agp1-M15Δ9N, and Agp1-M15Δ18N, dimer formation is stronger in the Pfr form than in the Pr form (Figure 6). This conformation-dependent dimerization of phytochrome fragments, which was also found for Cph1 (*29*), might provide a clue to understanding intramolecular signal transduction in phytochromes.

The histidine kinase has a negative impact on the dark stability of Pfr, as shown by the comparison of Agp1-FL and Agp1-M15 (Figure 4). It has been found that dark reversion of plant phytochrome depends on dimer formation (*43*). In these experiments, the Pfr form was more stable in the Pfr−Pfr homodimer than in the Pfr−Pr or Pfr−apoprotein heterodimers. The faster dark reversion of Agp1-FL as compared to that of Agp1-M15 might indicate that the interaction between chromophore module subunits is stronger in Agp1-M15 than in the full-length protein, where the histidine kinase might keep both chromophore modules in a different orientation with respect to each other.

Hinge Region. Limited proteolysis shows that in Agp1, the hinge region between the histidine kinase and the chromophore module becomes specifically exposed in the Pfr form. A similar but less pronounced effect has been found for cyanobacterial Cph1 (*29*). In plant phytochromes, the hinge region is also more exposed in the Pfr form than in the Pr form (*26*). For *Arabidopsis* phytochrome B, the PHY

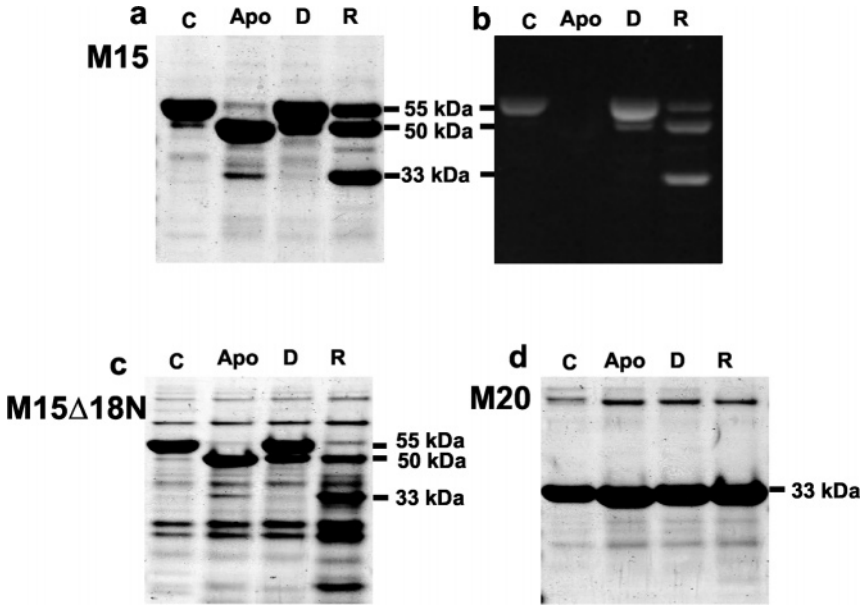

FIGURE 9: Proteolysis of Agp1-M15 (a and b), Agp1-M15Δ18N (c), and Agp1-M20 (d) with V8. In panels a and b, Coomassie stain and Zn^{2+}-induced fluorescence of the same SDS−PAGE gel are showm, respectively; in panels c and d, only Coomassie stains of SDS−PAGE gels are shown. The lanes and the sizes of protein fragments are labeled as in Figure 8a.

domain has been shown to interact with the double-PAS domain specifically in the Pr form (*27*). The exposure of the hinge region in the Pfr form of plant phytochromes might reflect the weakened interaction between both parts of the protein. However, the double-PAS domain is lacking in bacterial phytochromes. In these phytochromes, the PHY domain could protect the hinge region in the Pr form by an interaction with a part of the histidine kinase module. Alternatively, the hinge region could be protected in the Pr form by the tight interaction with the other subunit within the dimer. Both ideas are consistent with the BphP4 model (*34*), in which the exact position of the hinge region is, however, not resolved.

PHY Domain. For several phytochromes, including Agp1, the PHY domain has been reported to be specifically required for the formation of spectrally integer Pfr (*23*, *31*, *39*). This function is supported by the spectroscopic data presented here for Agp1-M20, which lacks the PHY domain (Figure 2). Whereas the spectrum of Agp1-M20 after dark assembly resembles that of Pr of Agp1-M15 and Agp1-FL, the photoproduct spectrum differs from that of Pfr, as the absorbance of the Q-band is diminished. The photoproduct spectrum resembles that of the cryotrapped meta-Rc intermediate of Agp1 (*11*). One plausible assumption for the spectral properties of Agp1-M20 is that the photoconversion of this fragment is arrested in an intermediate stage. In addition, these experiments revealed further information about functions of the PHY domain of Agp1. The slow assembly of Agp1-M20 (Figure 2) shows that the PHY domain is important for chromophore incorporation and plays thus a role in the formation of Pr. The cross-linking data imply that the PHY domain interacts with Lys 16, which is between the N-terminus and the chromophore-binding Cys 20. An intramolecular cross-link was found with Agp1-M15 and Agp1-M15Δ9N, but not with Agp1-M20 and Agp1-M15Δ18N (Figure 6). The PHY domain is also required for protein conformational changes that lead to the light-dependent subunit interaction. Agp1-M15 exhibited the largest SEC differences between the nonirradiated and photoconverted form (Figure 5b) and the most significant light effect on dimer cross-linking (Figure 6b). With Agp1-M20, no light effect on dimer cross-linking was found. The SEC differences between the two forms (Figure 5c) are rather small and are probably related to protein conformational changes. For these reasons, the PHY domain could be the site which forms a Pfr-specific contact with the partner subunit. The lack of photoinduced dimer formation in Agp1-M20 may, however, also result from an incomplete photoconversion. Agp1-M15 mutants that have an incomplete photocycle are also unable to undergo light-induced SEC mobility changes (*15*).

Since a part of the PHY domain is more exposed in the Pfr form than in the Pr form (Figures 8), it is unlikely that this part of the PHY domain functions as a Pfr-dependent dimerization site. However, a protease cleavage site in the PHY domain of Cph1 was more exposed in the Pr form than in the Pfr form (*29*).

PLD and GAF Domain. Agp1-M20 contains the PLD and GAF domains and the region N-terminal of the chromophore binding site. The Agp1-M20 fragment is comparable with the CBD of DrBphP which has been used for the determination of the crystal structure (*31*). We have found that, in contrast to the longer fragments, Agp1-M20 is resistant to V8 and trypsin proteolysis (Figure 9d and data not shown) and appears as a compact protein. The unit of PLD and GAF domains might be regarded as the core of BV-binding phytochromes, which contains the minimal elements that are required for chromophore incorporation and photoconversion. In our cross-linking experiments, we showed that Agp1-M20 can also form dimers (Figure 6c). As noted above, however, there was no evidence of a light effect on dimerization.

N-Terminal Amino Acids. Our experiments have shown that none of the amino acids between the N-terminus and the chromophore binding site are required for chromophore assembly. Agp1-M15Δ18N incorporated the chromophore at rates comparable with that of Agp1-FL/M15. Amino acids

FIGURE 10: Model for the protein conformation of Agp1 in the Pr and Pfr forms. The model was drawn assuming the following. (i) The N-terminal part (Nterm) and the PHY domain interact with each other. (ii) Two subunits form a dimer, mediated by the C-terminal histidine kinase (His kinase) module. (iii) Both chromophore modules (N-terminal part including the PHY domain) within the dimer interact stronger with each other in the Pfr form than in the Pr form. In this way, these parts of each monomer move closer to each other. (iv) The regions that are denoted with the arrows are specifically exposed in the Pfr form as shown by V8 and trypsin proteolysis. (v) The histidine kinase is weaker in the Pfr form than in the Pr form, because the distance between both subunits is increased upon photoconversion.

2−10 are not conserved among phytochromes. In Agp1, these amino acids play no role in the spectral properties but affect dark reversion and are involved in oligomer formation. Among these nine amino acids, there are two (negatively charged) Glu and two (positively charged) Arg residues; these amino acids might mediate the interaction of several subunits by ionic forces.

Amino acids 11−19, which are more conserved among phytochromes, are important for the proper formation of Pfr. The absorption spectrum of Agp1-M15Δ18N after assembly is comparable with that of proteins with an integer N-terminus. However, the photoproduct spectrum of Agp1-M15Δ18N is rather comparable with that of Agp1-M20 in the Q-band region (Figure 3). Despite the spectral aberration, Agp1-M15Δ18N undergoes protein conformational changes and also reveals a light effect on dimerization.

Model for Protein Conformational Changes during the Photoconversion of Agp1. The data obtained here by protein cross-linking, size exclusion chromatography, and limited proteolysis culminated in a model of the topography of Agp1 domains in the Pr and the Pfr form which is presented in Figure 10. The N-terminal chromophore modules, covering the PLD, the GAF domain, and the PHY domain, interact more tightly with each other upon photoconversion. Since this kind of light-induced subunit interaction has been found for Cph1 (*29*, *30*) and Agp1 (this work), which are rather distantly related (*19*), these results might point to a more universal mechanism of phytochrome photoconversion. The Pfr-dependent subunit interaction of the N-termini might lead to an increased distance between both histidine kinase subunits, thereby decreasing the kinase activity. The exposure of the hinge region in the Pfr form might be an indication of such a regulation. Histidine kinases are part of many bacterial sensory proteins. Although the modulation of histidine kinase activity is not understood for any system, recent models of the regulation of kinase activity are based on modulated distances or symmetries between both subunits within the dimer (*44*, *45*).

ACKNOWLEDGMENT

We thank Berthold Borucki, Maarten Heyn, and Sven Seibeck (Physics Department, Freie Universität Berlin) and members of the Sfb 498 for helpful discussions.

REFERENCES

1. Rockwell, N. C., and Lagarias, J. C. (2006) The structure of phytochrome: A picture is worth a thousand spectra, *Plant Cell 18*, 4−14.
2. Kendrick, R. E., and Kronenberg, G. H. M. (1994) *Photomorphogenesis in Plants*, 2nd ed., Kluwer Academic Publishers, Dordrecht, The Netherlands.
3. Giraud, E., Fardoux, J., Fourrier, N., Hannibal, L., Genty, B., Bouyer, P., Dreyfus, B., and Vermeglio, A. (2002) Bacteriophytochrome controls photosystem synthesis in anoxygenic bacteria, *Nature 417*, 202−205.
4. Giraud, E., Hannibal, L., Fardoux, J., Jaubert, M., Jourand, P., Dreyfus, B., Sturgis, J. N., and Vermeglio, A. (2004) Two distinct crt gene clusters for two different functional classes of carotenoid in *Bradyrhizobium*, *J. Biol. Chem. 279*, 15076−15083.
5. Goodner, B., Hinkle, G., Gattung, S., Miller, N., Blanchard, M., Qurollo, B., Goldman, B. S., Cao, Y., Askenazi, M., Halling, C., Mullin, L., Houmiel, K., Gordon, J., Vaudin, M., Iartchouk, O., Epp, A., Liu, F., Wollam, C., Allinger, M., Doughty, D., Scott, C., Lappas, C., Markelz, B., Flanagan, C., Crowell, C., Gurson, J., Lomo, C., Sear, C., Strub, G., Cielo, C., and Slater, S. (2001) Genome sequence of the plant pathogen and biotechnology agent *Agrobacterium tumefaciens* C58, *Science 294*, 2323−2328.
6. Wood, D. W., Setubal, J. C., Kaul, R., Monks, D. E., Kitajima, J. P., Okura, V. K., Zhou, Y., Chen, L., Wood, G. E., Almeida, N. F. J., Woo, L., Chen, Y., Paulsen, I. T., Eisen, J. A., Karp, P. D., Bovee, D. S., Chapman, P., Clendenning, J., Deatherage, G., Gillet, W., Grant, C., Kutyavin, T., Levy, R., Li, M. J., McClelland, E., Palmieri, A., Raymond, C., Rouse, G., Saenphimmachak, C., Wu, Z., Romero, P., Gordon, D., Zhang, S., Yoo, H., Tao, Y., Biddle, P., Jung, M., Krespan, W., Perry, M., Gordon-Kamm, B., Liao, L., Kim, S., Hendrick, C., Zhao, Z. Y., Dolan, M., Chumley, F., Tingey, S. V., Tomb, J. F., Gordon, M. P., Olson, M. V., and Nester, E. W. (2001) The genome of the natural genetic engineer *Agrobacterium tumefaciens* C58, *Science 294*, 2317−2323.
7. Lamparter, T., Michael, N., Caspani, O., Miyata, T., Shirai, K., and Inomata, K. (2003) Biliverdin binds covalently to *Agrobacterium* phytochrome Agp1 via its ring A vinyl side chain, *J. Biol. Chem. 278*, 33786−33792.
8. Karniol, B., and Vierstra, R. D. (2003) The pair of bacteriophytochromes from *Agrobacterium tumefaciens* are histidine kinases with opposing photobiological properties, *Proc. Natl. Acad. Sci. U.S.A. 100*, 2807−2812.
9. Karniol, B., and Vierstra, R. D. (2004) The HWE histidine kinases, a new family of bacterial two-component sensor kinases with potentially diverse roles in environmental signaling, *J. Bacteriol. 186*, 445−453.
10. Lamparter, T., Carrascal, M., Michael, N., Martinez, E., Rottwinkel, G., and Abian, J. (2004) The biliverdin chromophore binds covalently to a conserved cysteine residue in the N-terminus of *Agrobacterium* phytochrome Agp1, *Biochemistry 43*, 3659−3669.
11. Borucki, B., von Stetten, D., Seibeck, S., Lamparter, T., Michael, N., Mroginski, M. A., Otto, H., Murgida, D. H., Heyn, M. P., and Hildebrandt, P. (2005) Light-induced proton release of phytochrome is coupled to the transient deprotonation of the tetrapyrrole chromophore, *J. Biol. Chem. 280*, 34358−34364.
12. Inomata, K., Hammam, M. A. S., Kinoshita, H., Murata, Y., Khawn, H., Noack, S., Michael, N., and Lamparter, T. (2005) Sterically locked synthetic bilin derivatives and phytochrome Agp1 from *Agrobacterium tumefaciens* form photoinsensitive Pr- and Pfr-like adducts, *J. Biol. Chem. 280*, 24491−24497.
13. Inomata, K., Noack, S., Hammam, M. A. S., Khawn, H., Kinoshita, H., Murata, Y., Michael, N., Scheerer, P., Krauss, N., and Lamparter, T. (2006) Assembly of synthetic locked chromophores with *Agrobacterium* phytochromes Agp1 and Agp2, *J. Biol. Chem. 281*, 28162−28173.
14. Scheerer, P., Michael, N., Park, J. H., Noack, S., Förster, C., Hammam, M. A. S., Inomata, K., Choe, H. W., Lamparter, T., and Krauss, N. (2006) Crystallization and preliminary X-ray crystallographic analysis of the N-terminal photosensory module of phytochrome Agp1, a biliverdin-binding photoreceptor from *Agrobacterium tumefaciens*, *J. Struct. Biol. 153*, 97−102.
15. von Stetten, D., Seibeck, S., Michael, N., Scheerer, P., Mroginski, M. A., Murgida, D. H., Krauss, N., Heyn, M. P., Hildebrandt, P., Borucki, B., and Lamparter, T. (2007) Highly conserved residues

D197 and H250 in Agp1 phytochrome control the proton affinity of the chromophore and Pfr formation, *J. Biol. Chem. 282*, 2116−2123.
16. Oberpichler, I., Molina, I., Neubauer, O., and Lamparter, T. (2006) Phytochromes from *Agrobacterium tumefaciens*: Difference spectroscopy with extracts of wild type and knockout mutants, *FEBS Lett. 580*, 437−442.
17. Ponting, C. P., and Aravind, L. (1997) PAS: A multifunctional domain family comes to light, *Curr. Biol. 7*, R674−R677.
18. Aravind, L., and Ponting, C. P. (1997) The GAF domain: An evolutionary link between diverse phototransducing proteins, *Trends Biochem. Sci. 22*, 458−459.
19. Lamparter, T. (2004) Evolution of cyanobacterial and plant phytochromes, *FEBS Lett. 573*, 1−5.
20. Lamparter, T., Michael, N., Mittmann, F., and Esteban, B. (2002) Phytochrome from *Agrobacterium tumefaciens* has unusual spectral properties and reveals an N-terminal chromophore attachment site, *Proc. Natl. Acad. Sci. U.S.A. 99*, 11628−11633.
21. Tasler, R., Moises, T., and Frankenberg-Dinkel, N. (2005) Biochemical and spectroscopic characterization of the bacterial phytochrome of *Pseudomonas aeruginosa*, *FEBS Lett. 272*, 1927−1936.
22. Blumenstein, A., Vienken, K., Tasler, R., Purschwitz, J., Veith, D., Frankenberg-Dinkel, N., and Fischer, R. (2005) The *Aspergillus nidulans* phytochrome FphA represses sexual development in red light, *Curr. Biol. 15*, 1833−1838.
23. Karniol, B., Wagner, J. R., Walker, J. M., and Vierstra, R. D. (2005) Phylogenetic analysis of the phytochrome superfamily reveals distinct microbial subfamilies of photoreceptors, *Biochem. J. 392*, 103−116.
24. Giraud, E., Zappa, S., Jaubert, M., Hannibal, L., Fardoux, J., Adriano, J. M., Bouyer, P., Genty, B., Pignol, D., and Vermeglio, A. (2004) Bacteriophytochrome and regulation of the synthesis of the photosynthetic apparatus in *Rhodopseudomonas palustris*: Pitfalls of using laboratory strains, *Photochem. Photobiol. Sci. 3*, 587−591.
25. Nakasako, M., Wada, M., Tokutomi, S., Yamamoto, K. T., Sakai, J., Kataoka, F., and Furuya, M. (1990) Quaternary structure of pea phytochrome I dimer studied with small-angle X-ray scattering and rotary-shadowing electron microscopy, *Photochem. Photobiol. 52*, 3−12.
26. Song, P. S. (1999) Inter-domain signal transmission within the phytochromes, *J. Biochem. Mol. Biol. 31*, 215.
27. Chen, M., Tao, Y., Lim, J., Shaw, A., and Chory, J. (2005) Regulation of phytochrome B nuclear localization through light-dependent unmasking of nuclear-localization signals, *Curr. Biol. 15*, 637−642.
28. Otto, H., Lamparter, T., Borucki, B., Hughes, J., and Heyn, M. P. (2003) Dimerization and inter-chromophore distance of Cph1 phytochrome from *Synechocystis*, as monitored by fluorescence homo and hetero energy transfer, *Biochemistry 42*, 5885−5895.
29. Esteban, B., Carrascal, M., Abian, J., and Lamparter, T. (2005) Light-induced conformational changes of cyanobacterial phytochrome Cph1 probed by limited proteolysis and autophosphorylation, *Biochemistry 44*, 450−461.
30. Strauss, H. M., Schmieder, P., and Hughes, J. (2005) Light-dependent dimerisation in the N-terminal sensory module of cyanobacterial phytochrome 1, *FEBS Lett. 579*, 3970−3974.
31. Wagner, J. R., Brunzelle, J. S., Forest, K. T., and Vierstra, R. D. (2005) A light-sensing knot revealed by the structure of the chromophore-binding domain of phytochrome, *Nature 438*, 325−331.
32. Heyne, K., Herbst, J., Stehlik, D., Esteban, B., Lamparter, T., Hughes, J., and Diller, R. (2002) Ultrafast dynamics of phytochrome from the cyanobacterium *Synechocystis*, reconstituted with phycocyanobilin and phycoerythrobilin, *Biophys. J. 82*, 1004−1016.
33. van Thor, J. J., Borucki, B., Crielaard, W., Otto, H., Lamparter, T., Hughes, J., Hellingwerf, K. J., and Heyn, M. P. (2001) Light-induced proton release and proton uptake reactions in the cyanobacterial phytochrome Cph1, *Biochemistry 40*, 11460−11471.
34. Evans, K., Grossmann, J. G., Fordham-Skelton, A. P., and Papiz, M. Z. (2006) Small-angle X-ray scattering reveals the solution structure of a bacteriophytochrome in the catalytically active Pr state, *J. Mol Biol.* (in press).
35. Jones, A. M., and Quail, P. H. (1986) Quaternary structure of 124-kilodalton phytochrome from *Avena sativa* L, *Biochemistry 25*, 2987−2995.
36. Sineshchekov, V., Koppel', L., Esteban, B., Hughes, J., and Lamparter, T. (2002) Fluorescence investigation of the recombinant cyanobacterial phytochrome (Cph1) and its C-terminally truncated monomeric species (Cph1Δ2): Implication for holoprotein assembly, chromophore-apoprotein interaction and photochemistry, *J. Photochem. Photobiol., B 67*, 39−50.
37. Mancinelli, A. (1994) The physiology of phytochrome action, in *Photomorphogenesis in Plants* (Kendrick, R. E., and Kronenberg, G. H. M., Eds.) 2nd ed., pp 211−269, Kluwer Academic Publishers, Dordrecht, The Netherlands.
38. Berkelman, T. R., and Lagarias, J. C. (1986) Visualization of bilin-linked peptides and proteins in polyacrylamide gels, *Anal. Biochem. 156*, 194−201.
39. Oka, Y., Matsushita, T., Mochizuki, N., Suzuki, T., Tokutomi, S., and Nagatani, A. (2004) Functional analysis of a 450-amino acid N-terminal fragment of phytochrome B in *Arabidopsis*, *Plant Cell 16*, 2104−2116.
40. Kneip, C., Schlamann, W., Braslavsky, S. E., Hildebrandt, P., and Schaffner, K. (2000) Resonance Raman spectroscopic study of the tryptic 39-kDa fragment of phytochrome, *FEBS Lett. 482*, 252−256.
41. Reiff, U., Eilfeld, P., and Rüdiger, W. (1985) A photoreversible 39-kdalton fragment from the Pfr form of 124-kdalton oat phytochrome, *Z. Naturforsch. C 40*, 693−698.
42. Lagarias, J. C., and Mercurio, F. M. (1985) Structure function studies on phytochrome. Identification of light-induced conformational changes in 124-kDa *Avena* phytochrome in vitro, *J. Biol. Chem. 260*, 2415−2423.
43. Hennig, L., and Schäfer, E. (2001) Both Subunits of the Dimeric Plant Photoreceptor Phytochrome Require Chromophore for Stability of the Far-red Light-absorbing Form, *J. Biol. Chem. 276*, 7913−7918.
44. Khorchid, A., and Ikura, M. (2006) Bacterial histidine kinase as signal sensor and transducer, *Int. J. Biochem. Cell Biol. 38*, 307−312.
45. Neiditch, M. B., Federle, M. J., Pompeani, A. J., Kelly, R. C., Swem, D. L., Jeffrey, P. D., Bassler, B. L., and Hughson, F. M. (2006) Ligand-induced asymmetry in histidine sensor kinase complex regulates quorum sensing, *Cell 126*, 1095−1108.

BI602419X